Simultaneous near infrared photothermal therapy and temperature mapping by magnetic resonance in 3D cell aggregates loaded with Fe_3Se_4 nanoparticles

Joana F. Soeiro[1,2], Rute A. Pereira[1,2], Rui Oliveira-Silva[1,2], Filipa L. Sousa[2], Vítor M. Gaspar[2], João F. Mano[2], Ángel Millán[3], Claudia Innocenti[4,5], Manuel Mariani[6,7], Alessandro Lascialfari[6,7], Nuno J. O. Silva[1,2*]

[1*]Department of Physics and CICECO - Aveiro Institute of Materials , University of Aveiro, Campus Universitário de Santiago, Aveiro, 3810-193, Portugal.
[2*]Department of Chemistry and CICECO - Aveiro Institute of Materials , University of Aveiro, Campus Universitário de Santiago, Aveiro, 3810-193, Portugal.
[3]Institute of Nanoscience and Materials of Aragon (INMA), CSIC-University of Zaragoza, Zaragoza, 50009, Spain.
[4]Dipartimento di Chimica, Università di Firenze and INSTM, 50019 Sesto Fiorentino (FI), Italy.
[5]ICCOM-CNR, 50019 Sesto Fiorentino (FI), Italy.
[6]INFN, Istituto Nazionale di Fisica Nucleare, Pavia, Italy.
[7]Department of Physics University of Pavia, Pavia, Italy.

*Corresponding author(s). E-mail(s): nunojoao@ua.pt;
Contributing authors: joana.soeiro@ua.pt; rute.pereira@ua.pt; ruipedro.silva@ua.pt; filipalsousa@ua.pt; vm.gaspar@ua.pt; jmano@ua.pt; amillan@unizar.es; claudia.innocenti@unifi.it; manuel.mariani@unipv.it; alessandro.lascialfari@unipv.it;

Abstract

Control over temperature in space and time is of utmost importance in many contexts, including photothermal therapies, where a good temperature monitoring and control is expected to improve their clinical outcome. One of the most promising techniques involves the use of magnetic resonance imaging, exploring the temperature change of proton relaxometric properties or exploring the temperature change of contrast agents. In real applications, the use of contrast agents for thermometry is much better justified if thermometry comes as an added value of a photothermal agent. Here we show iron selenide nanoparticles (NPs) that are able to work simultaneously as efficient near infrared photothermal and thermometry agents embedded in cellular models at concentrations where their toxicity is low. The simultaneous heat generation and temperature mapping around these NPs allow the control over the depth achieved by the therapy and detection and control of hot spots that would be otherwise overlooked, for instance.

Keywords: simultaneous heat generation and temperature mapping, magnetic resonance imaging thermometry, near infrared heating, cellular hyperthermia

1 Introduction

Heat generation and thermometry are two complementary aspects of hyperthermia therapies that are hard to combine. On one hand, there is a quest for thermal agents with improved heat generation ability and, on the other hand there is a quest for temperature sensing and mapping with improved space and time resolution, and temperature sensitivity. Efforts to combine both include laser heating with optical thermometry,[1] magnetic heating with optical thermometry,[2, 3] magnetic heating with magnetic particle imaging (MPI) thermometry,[4, 5] and laser heating with magnetic resonance imaging (MRI) thermometry.[6] Optical thermometry has an excellent space resolution but it has intrinsic limitations for in-depth sensing, which prevents its application in many clinical applications.[7] This can be partially overcome by shifting the sensing to the infrared but in this case sensing and heating overlap, with the heating hindering the sensing counterpart. MPI thermometry is expected to be useful when combined with magnetic hyperthermia since there is evidence that both the magnetic hyperthermia and MPI equipment can be combined.[4] In the case of MRI thermometry, the best combination is with optical hyperthermia, since no cross-interference is observed.[8] MRI thermometry is based on the intrinsic variation of contrast parameters with temperature, such as proton resonance frequency and longitudinal and transverse relaxation times. The advantage of using intrinsic variation is that it is a totally noninvasive technique, while the disadvantage is the small variation of contrast with temperature.[6] Larger temperature variations can be obtained with the use of contrast agents, with the clear disadvantage of making MRI thermometry an invasive technique.[9] The idea of using contrast agents with a magnetic phase transition around body temperature as a way to obtain a large variation of the magnetic response (and thus contrast)

around that temperature emerged back in the '90s, with the first example being a millimetric piece of metallic gadolinium with a transition temperature of 18 °C.[10] Clearly, the practical application of this example is limited and an improved version with micrometric particles appeared later.[11] Anyway, it is quite difficult to make smaller (nanosized) metallic gadolinium particles, as they undergo a spontaneous oxidation upon exposure to air ambient conditions,[12] and it is not clear how to increase their transition temperature from 18 °C to $\sim$ 42 °C, which is required for clinical applications. More recently, manganese, cobalt, and zinc ferrites appeared as an option, with the advantage of tuning the transition temperature by doping.[13–16] However, having simultaneously isolated NPs and a large decrease of the magnetic response with temperature is proving difficult: in agglomerates of nanocrystals the decrease of magnetization with temperature is high, leading to a good temperature sensitivity, but when isolated NPs are obtained, the decrease of magnetization is much smaller.[17] We believe that this is associated with the fact that nanosized magnetic systems have a transition temperature broadened due to surface effects,[18] and that this broadening is more dramatic in low anisotropy materials such as ferrites, since the magnetic transitions are broader in 3D latices of low anisotropy (Heisenberg) spins, when compared with 3D latices of high anisotropy (Ising) spins (see, for instance [19]).

Despite the improvement in sensitivity provided by contrast agents, in real clinical practice, the use of thermometric contrast agents must be carefully considered in terms of a risk/benefit balance. This balance is expected to increase dramatically towards the benefit side in situations where the use of a photothermal agent is needed. In such cases, the thermometric feature would be regarded as a great added value to an already needed invasive practice. Here we show isolated and functionalized NPs that combine low cytotoxicity, good efficiency in the 1^{st} and 2^{nd} windows of near infrared (NIR) hyperthermia, and a high magnetic anisotropy granting an excellent thermometric response that can be imaged in an MRI in the temperature window used in clinical NIR hyperthermia. The combination of these three pillars - low cytotoxicity, good photo-thermal efficiency and high-temperature sensitivity - in isolated NPs is critical for a formulation able to eventually reach the market of photo-thermal-contrast agents.

2 Results and discussion

The particles here reported are iron selenide (Fe_3Se_4) NPs with a rhombohedral shape and an average size of 170 $\pm$ 10 nm (see SI, Fig. S3, S4 and S5). The production of pure Fe_3Se_4 NPs requires a delicate tuning of parameters such as temperature, temperature ramp, precursors, solvent, and stabilizing agents, since other phases ($FeSe_2$ and FeSe) may also nucleate and grow. Here we explore the production of Fe_3Se_4 NPs using a simpler route, when compared to the current state-of-the-art.[20] The route here presented involves the use of iron acetate and selenium-octadecene as precursors, the use of octadecene as the solvent, tetradecylphosphonic acid and 1-Dodecanethiol as stabilizing agents, and the thermaldecomposition of the precursors into the NPs at 250 °C with an heating ramp of 5 °C/min. Such a thermodecomposition route in organic media has the

benefit of producing isolated and better controlled NPs and the drawback of producing them with an hydrophobic surface, such that an extra phase-transfer step is needed for their use in cellular medium. To this aim, we explored the use of caffeic acid and dopamine, which are molecules with catechol groups that are expected to interact with the iron atoms located at the surface of the NPs, as previously found in Fe_3Se_4 [20] and Fe_3O_4 [21]. The final result is hydrophilic NPs with reactive amine or carboxyl groups, ready to be dispersed in cell culture media and explored as a photothermal and thermometric agent in cells.

As mentioned in the introduction, the first pillar on which a good photothermal-contrast agent stands is low cytotoxicity. This was accessed using the AlamarBlue® assay up to 72 h after NPs being incubated with L929 cells. Cells remained viable (>85 %) for all the time points tested for the incubation concentration range of 0 - 500 $\mu g\,mL^{-1}$ of NPs (Fig. 1a). Consequently, it is possible to use incubation concentrations in this range for the remaining studies involving simultaneous NIR hyperthermia and MRI thermometry in cell pellets.

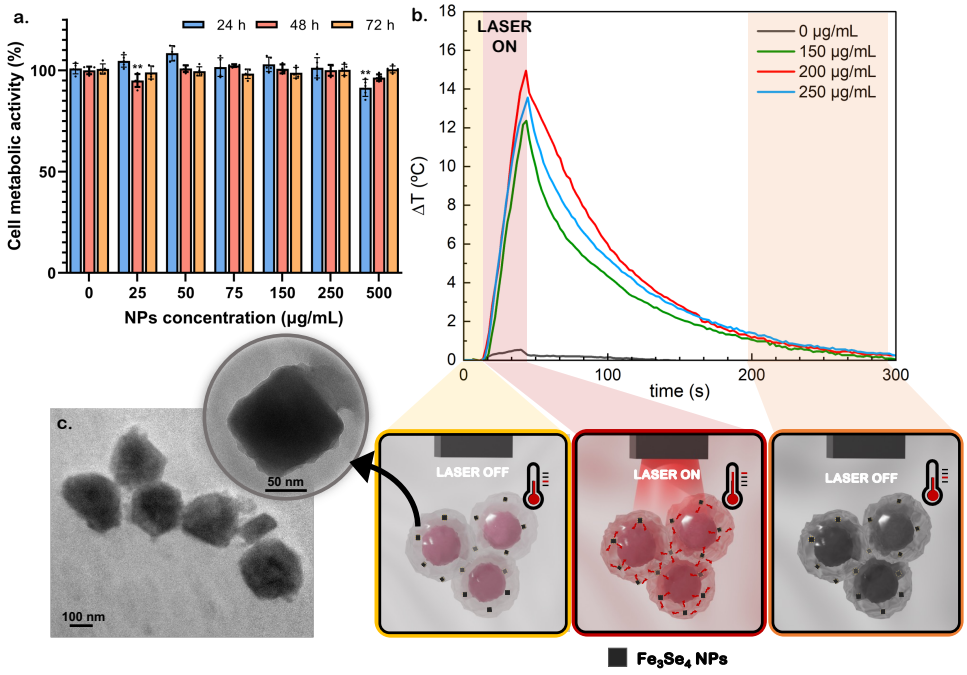

Fig. 1 (a) Evaluation of L929 metabolic activity up to 72 h after cells being incubated with Fe_3Se_4 NPs. Data are represented as mean ± s.d. (n = 5), **p<0.05; (b) Heating curves of the cell samples with Fe_3Se_4 NPs at different incubation concentrations, obtained with a 808 nm laser at power density of 1.48 $W\,cm^{-2}$ for 30 s; and (c) Transmission Electron Microscopy images of Fe_3Se_4 NPs.

The Fe_3Se_4 NPs have a strong absorption in a broad range from UV, to visible light, to NIR, including in the two relevant optical windows of tissues (see SI, Fig. S6). The heating ability of Fe_3Se_4 NPs at 808 nm in the cellular samples was accessed in the NPs incubation concentration range of 0 - 250 $\mu g\,mL^{-1}$ with a laser at power density of 1.48 $W\,cm^{-2}$ for 30 s. This NIR dose resulted in a temperature increase between 12 °C to 15 °C, depending on the NPs incubation concentration (Fig. 1b). The maximum SAR value estimated from the initial slope of the time-temperature curves was 80 $W\,g^{-1}$ for the sample with a NPs incubation concentration of 150 $\mu g\,mL^{-1}$ (see SI, Fig. S7). These results show the ability of Fe_3Se_4 NPs as photothermal agents.

At the core of the temperature sensitivity observed in MRI is an order-disorder magnetic phase transition observed in Fe_3Se_4 NPs at around 40 °C (Fig. 2(a)), a temperature that makes these NPs suitable for sensing in the context of bio-applications. This magnetic phase transition is quite immune to surrounding parameters other than temperature, such as viscosity, pH, and saline concentration, making magnetic NPs with such a phase transition particularly suitable for temperature sensing. The magnetic phase transition is associated with a strong decrease of the net magnetic moment of each NP. This net magnetic moment is the vector sum of the magnetic moments of all Fe^{2+} and Fe^{3+} ions of the NP, being well ordered at low temperature. When approaching 40 °C, their fluctuation increases and their long-range (intra-NP) order is lost, resulting in the above-mentioned decrease of the net magnetic moment of each NP. The net magnetic moment is responsible for creating a dipolar magnetic field that disturbs the relaxation of the spins of the surrounding protons: the higher this disturbance is, the more "efficient" the contrast agent is expected to be, being this "efficiency" measured as a longitudinal and transverse relaxivity (r_1 and r_2, respectively). It is thus expected that the decrease of the net magnetic moment with temperature leads to a decrease of the relaxivity. It was observed that the magnetic properties of the Fe_3Se_4 NPs did not undergo significant changes following functionalization (see SI, Fig. S8).

The obtained values of r_1 and r_2 with the cell samples with different NPs incubation concentrations (Fig.2(b) and Fig. S9) are modest when compared with benchmark NPs explored as simple non-thermometric contrast agents [22, 23] but, when comparing the obtained r_2/r_1 ratio (25.5 at 29 °C, 0.55 T, see SI Fig. S10), our particles have a good performance co andpared to other NPs that are commercially available as MRI T_2 contrast agents (which are in the range of 12 - 20 at 1.5 T [24]) and compared to other reported NPs (which are in the range of 13 - 26 at 1.5 T[24]). The r_2/r_1 ratio indicates how eligible for negative or positive contrast a contrast agent is. Usually, if the r2/r1 ratio is >10, the material is a good T_2 contrast agent [25]. Thus, the relaxivity of the Fe_3Se_4 NPs is enough to generate a contrast suitable for clinical applications. As temperature increases, r_2 decreases while r_1 increases, confirming the ability of the Fe_3Se_4 NPs to generate a temperature-dependent contrast, which is the base of MR thermometry based on contrast agents (Fig. 2(b) and Fig. S9).

The existence of a relevant variation of r_1 and r_2 with temperature opens the possibility to obtain MRI images with temperature-dependent intensity when exploring sequences weighted in T_1 or T_2. In fact, T_2 weighted gradient echo (GE) images obtained with temperature (where the temperature of the samples was

increased in a controlled way) in cell pellets loaded with Fe_3Se_4 NPs show a temperature-dependent increase of intensity up to $5.9\,\%\,°C^{-1}$ and $8.8\,\%\,°C^{-1}$, for the samples with NPs incubation concentration of $150\,\mu g\,mL^{-1}$ and $200\,\mu g\,mL^{-1}$, respectively, while the control sample without NPs had an intensity decrease up to $1.2\,\%\,°C^{-1}$ (Fig. 2c and Fig. S11). The relative image intensity of the GE images, representing the ratio between the control sample and samples with NPs, are presented in Fig. 2d. Similarly as observed in another reported studies [11, 13, 15, 16], the relative image intensity increases with NPs concentration and decreases with temperature.

The controlled temperature experiments allows to establish a calibration curve for each NPs incubation concentration based on the relation between intensity and temperature (see SI, Fig. S11). In the temperature-controlled experiments, taking a one-point optical thermometer as reference, a good accuracy was obtained in the temperature range between 30 and 45 °C ($< 1\,°C$), when comparing the "real" temperature value, measured with the optical thermometer, and the temperature measured with our calibration method (see SI, Fig. S14). The obtained accuracy is similar to the values reported in other studies.[11, 13, 15, 16]

The validation of the NPs low cytotoxicity and their incorporation in 3D cell pellets mimicking tissues, together with the validation of a good photo-thermal efficiency and high temperature sensitivity in a single nanoparticle system, opens the way for a real-time temperature mapping of the non-controlled temperature increase in the 3D cell pellets under NIR (Fig. 3, Fig. S15 and videos available as SI). Before the laser is turned on, the MRI intensity is fairly constant across the cell pellet and so does the temperature, as seen in the first frame of Fig. 3a and 3b, and in the first points of Fig. 3c and 3d (please see also SI Videos). As the laser is turned on, the average intensity increases steadily. A few seconds after the laser is turned on, an increase of temperature is readily detected on the top of the cell pellet (the region of incidence), expanding to regions farther away as time increase. After the laser is turned off, the temperature decreases back to a value close to the initial value, showing the reversibility of the system and the reversibility of the temperature sensing method. In other words, whatever changes occur in the cell pellet that can in principle contribute to a change in MRI intensity, like dehydration, changes in the density of protons or their environment, they do not have a relevant contribution to the image when compared to the dominant contribution of the temperature-dependent relaxivity of the Fe_3Se_4 NPs. When the average across the volume is taken, an increase from 31 °C to 57 °C is measured. However, this average hides transient temperature differences within the sample of more than 20 °C, since the top of the sample is constantly being irradiated during the heating time, differences that would be overlooked in a simple measurement with a thermocouple or equivalent. While the average reveals the exponential increase and decrease of temperature that is often observed and expected for a conduction mechanisms, the heat and the temperature maps provided by the Fe_3Se_4 NPs reveal the details of the temporal and space evolution of temperature and the details of its heterogeneity.

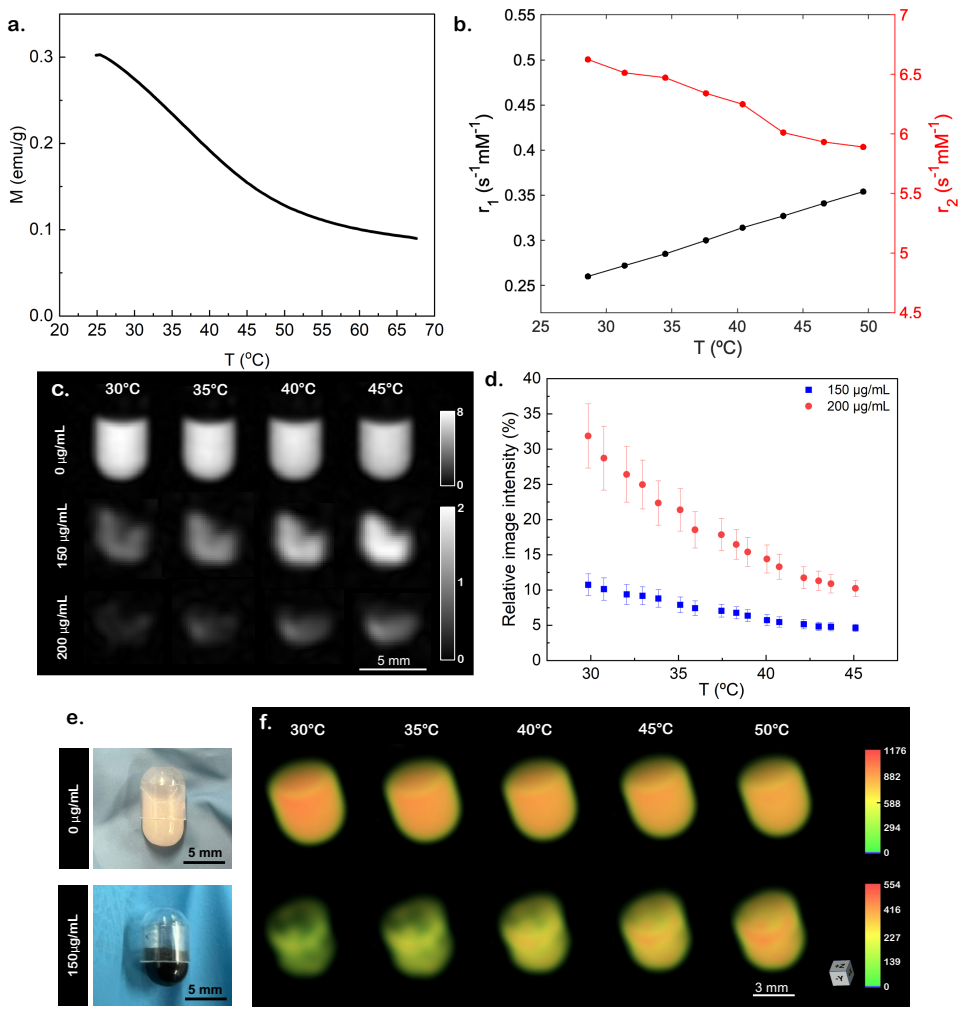

Fig. 2 (a) Dependence of the magnetization of Fe_3Se_4 NPs with temperature at 0.5 T; (b) Variation of r_1 and r_2 with temperature of the cell samples with Fe_3Se_4 NPs; (c) 2D GE images of cell samples with 150 and 200 μg mL^{-1} incubation concentration of NPs and without NPs over controlled temperature; (d) Relative image intensity variation of the 2D GE images of cell samples with NPs with temperature (data presented as average value ± s.d.); (e) Images of cell samples with and without NPs, and (f) 3D GE images of cell samples with (150 μg mL^{-1} incubation concentration) and without NPs over controlled temperature.

3 Conclusions

In summary, the Fe_3Se_4 NPs here reported open the way for a simultaneous and efficient local NIR cellular heating and temperature mapping in space and time. This enables temperature monitoring and control during laser photothermal therapy:

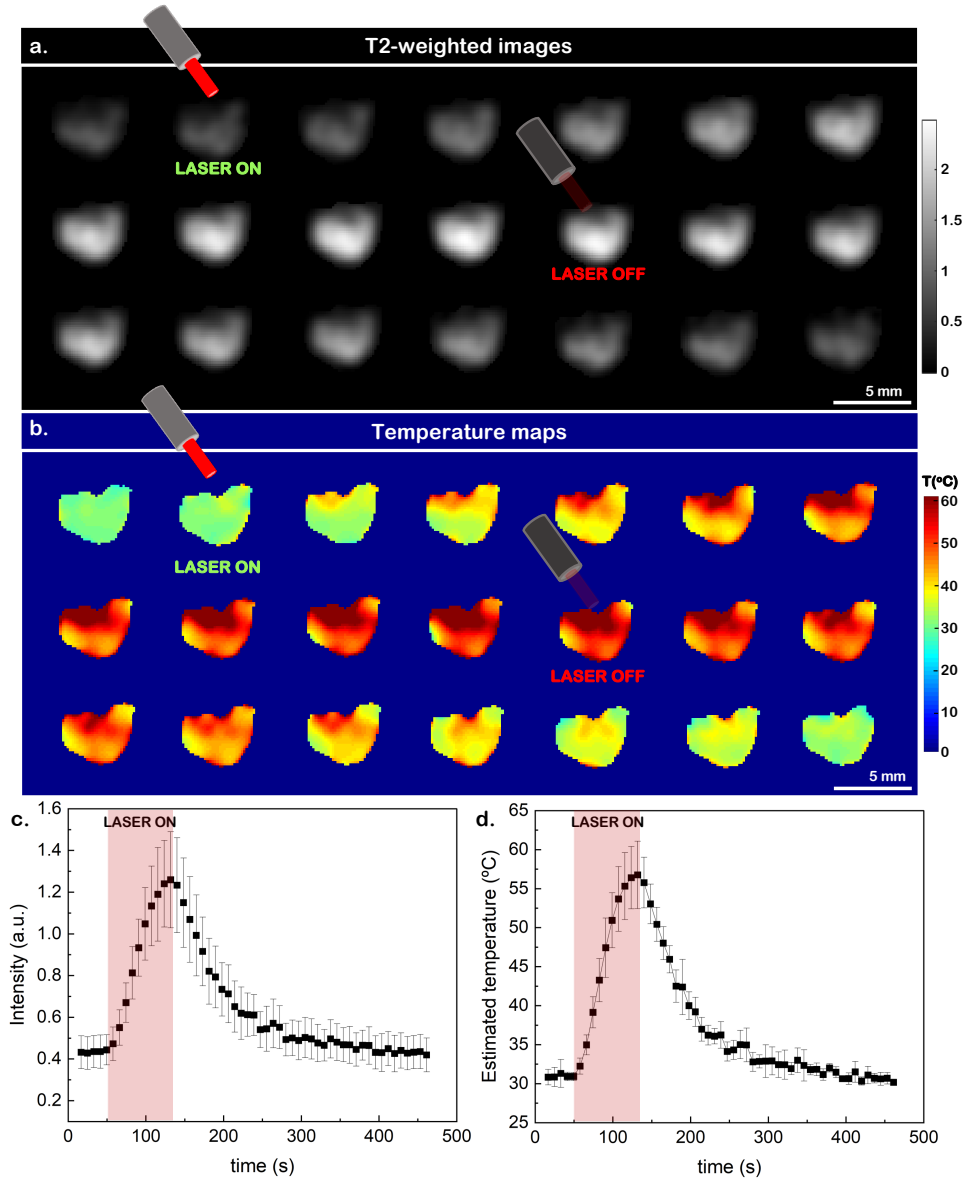

Fig. 3 (a) T_2-weighted images obtained with a cell sample (150 µg mL^{-1} incubation concentration of Fe_3Se_4 NPs) before, under NIR irradiation for 82 s at 0.67 W cm^{-2}, and after that irradiation (8 s integration time per image, pixel size of 0.16 mm); (b) Associated temperature maps determined through the obtained calibrations; (c) Variation with time of the average MRI intensity and (d) variation with time of the average temperature estimated from the intensity images (data presented as average value ± s.d.). Please see the SI Videos with the temporal evolution of the MR images and temperature maps.

control on the maximum achieved temperature, and control of the depth and extension of the therapy. The ultimate space, time resolution and temperature resolution are entangled and are constrained both by the Fe_3Se_4 NPs and the MRI scanner. The high temperature sensitivity presented by the Fe_3Se_4 NPs contributes to a good performance in all these resolutions. The combination of the two invasive thermal agents and contrast agents in a single agent is expected to widen the range of real situations where the benefit of the temperature-controlled thermal therapy overcomes its associated risks, opening to way to real applications of thermometric photothermal agents.

4 Acknowledgments

This research was funded by project CICECO – Aveiro Institute of Materials, UIDB/50011/2020 & UIDP/50011/2020, financed by national funds through the Portuguese Foundation for Science and Technology/MCTES. This work was also supported by the Programa Operacional Competitividade e Internacionalização (POCI), in the component FEDER, and by national funds (OE) through FCT/MCTES, in the scope of the projects PANGEIA (PTDC/BTM-SAL/30503/2017). The authors acknowledge the financial support by the Portuguese Foundation for Science and Technology (FCT) through the Doctoral Grants (2022.10039.BD, Joana Soeiro, SFRH/BD/143320/2019, Rute A. Pereira) and through an Assistant Researcher contract (DOI: 10.54499/2022.02106.CEECIND/CP1720/CT0028, Vítor M. Gaspar). Additionally, this work was supported by Grants PTDC/NAN-MAT/3901/2020 (DOI: 10.54499/PTDC/NAN-MAT/3901/2020 supported by POCI, FEDER and FCT/MCTES) and Grant ERC-2019-CoG-865437 from the European Research Council (ERC) under the European Union's Horizon 2020 research and innovation programme.

References

[1] Debasu, M. L. *et al.* All-in-one optical heater-thermometer nanoplatform operative from 300 to 2000 k based on er3+ emission and blackbody radiation. *Advanced Materials* **25**, 4868–4874 (2013).

[2] Pinol, R. *et al.* Joining time-resolved thermometry and magnetic-induced heating in a single nanoparticle unveils intriguing thermal properties. *ACS nano* **9**, 3134–3142 (2015).

[3] Gu, Y. *et al.* Local temperature increments and induced cell death in intracellular magnetic hyperthermia. *ACS nano* **17**, 6822–6832 (2023).

[4] Healy, S. *et al.* Clinical magnetic hyperthermia requires integrated magnetic particle imaging. *Wiley Interdisciplinary Reviews: Nanomedicine and Nanobiotechnology* **14**, e1779 (2022).

[5] Barrera, G., Allia, P. & Tiberto, P. Multifunctional effects in magnetic nanoparticles for precision medicine: combining magnetic particle thermometry and hyperthermia. *Nanoscale Advances* **5**, 4080–4094 (2023).

[6] Rieke, V. & Butts Pauly, K. Mr thermometry. *Journal of Magnetic Resonance Imaging: An Official Journal of the International Society for Magnetic Resonance in Medicine* **27**, 376–390 (2008).

[7] Zhou, J., Del Rosal, B., Jaque, D., Uchiyama, S. & Jin, D. Advances and challenges for fluorescence nanothermometry. *Nature methods* **17**, 967–980 (2020).

[8] Rodrigues, H. F., Capistrano, G. & Bakuzis, A. F. In vivo magnetic nanoparticle hyperthermia: A review on preclinical studies, low-field nano-heaters, noninvasive thermometry and computer simulations for treatment planning. *International Journal of Hyperthermia* **37**, 76–99 (2020).

[9] Zhu, M., Sun, Z. & Ng, C. K. Image-guided thermal ablation with mr-based thermometry. *Quantitative imaging in medicine and surgery* **7**, 356 (2017).

[10] Settecase, F., Sussman, M. & Roberts, T. A new temperature-sensitive contrast mechanism for mri: Curie temperature transition-based imaging. *Contrast Media & Molecular Imaging* **2**, 50–54 (2007).

[11] Hankiewicz, J., Celinski, Z., Stupic, K., Anderson, N. & Camley, R. Ferromagnetic particles as magnetic resonance imaging temperature sensors. *Nature communications* **7**, 12415 (2016).

[12] Nelson, J. A., Bennett, L. H. & Wagner, M. J. Solution synthesis of gadolinium nanoparticles. *Journal of the American Chemical Society* **124**, 2979–2983 (2002).

[13] Alghamdi, N. *et al.* Development of ferrite-based temperature sensors for magnetic resonance imaging: A study of cu 1- x zn x fe 2 o 4. *Physical review applied* **9**, 054030 (2018).

[14] Stroud, J. *et al.* Magnetic particle based mri thermometry at 0.2 t and 3 t. *Magnetic Resonance Imaging* **100**, 43–54 (2023).

[15] Hankiewicz, J. H. *et al.* Zinc doped copper ferrite particles as temperature sensors for magnetic resonance imaging. *Aip Advances* **7** (2017).

[16] Hankiewicz, J. H. *et al.* Nano-sized ferrite particles for magnetic resonance imaging thermometry. *Journal of Magnetism and Magnetic Materials* **469**, 550–557 (2019).

[17] Jang, J.-t. *et al.* Critical enhancements of mri contrast and hyperthermic effects by dopant-controlled magnetic nanoparticles. *Angewandte Chemie International Edition* **48**, 1234–1238 (2009).

[18] Shinjo, T., Kiyama, M., Sugita, N., Watanabe, K. & Takada, T. Surface magnetism of α-fe2o3 by mössbauer spectroscopy. *Journal of Magnetism and Magnetic Materials* **35**, 133–135 (1983).

[19] de Jongh, L. & Miedema, A. Experiments on simple magnetic model systems. *Advances in Physics* **23**, 1–260 (1974).

[20] Oliveira-Silva, R. *et al.* Temperature-responsive nanomagnetic logic gates for cellular hyperthermia. *Materials Horizons* **6**, 524–530 (2019).

[21] Liu, Y. *et al.* Facile surface functionalization of hydrophobic magnetic nanoparticles. *Journal of the American Chemical Society* **136**, 12552–12555 (2014).

[22] Vuong, Q. L., Berret, J.-F., Fresnais, J., Gossuin, Y. & Sandre, O. A universal scaling law to predict the efficiency of magnetic nanoparticles as mri t2-contrast agents. *Advanced healthcare materials* **1**, 502–512 (2012).

[23] Rohrer, M., Bauer, H., Mintorovitch, J., Requardt, M. & Weinmann, H.-J. Comparison of magnetic properties of mri contrast media solutions at different magnetic field strengths. *Investigative radiology* **40**, 715–724 (2005).

[24] Basly, B. *et al.* Effect of the nanoparticle synthesis method on dendronized iron oxides as mri contrast agents. *Dalton transactions* **42**, 2146–2157 (2013).

[25] Caspani, S., Magalhães, R., Araújo, J. P. & Sousa, C. T. Magnetic nanomaterials as contrast agents for mri. *Materials* **13**, 2586 (2020).